We are IntechOpen,
the world's leading publisher of Open Access books
Built by scientists, for scientists

4,800
Open access books available

122,000
International authors and editors

135M
Downloads

154
Countries delivered to

Our authors are among the

TOP 1%
most cited scientists

12.2%
Contributors from top 500 universities

BOOK CITATION INDEX
CLARIVATE ANALYTICS
INDEXED

WEB OF SCIENCE™

Selection of our books indexed in the Book Citation Index
in Web of Science™ Core Collection (BKCI)

Interested in publishing with us?
Contact book.department@intechopen.com

Numbers displayed above are based on latest data collected.
For more information visit www.intechopen.com

Theoretical Basis of Electrocatalysis

Chi Ho Lee and Sang Uck Lee

Additional information is available at the end of the chapter

http://dx.doi.org/10.5772/intechopen.77109

Abstract

In this chapter, we introduce the density functional theory (DFT)-based computational approaches to the study of various electrochemical reactions (hydrogen evolution reaction (HER), oxygen evolution reaction (OER), oxygen reduction reaction (ORR)) occurring on heterogeneous catalysis surfaces. A detailed computational approach to the theoretical interpretation of electrochemical reactions and structure-catalytic activity relationships for graphene-based catalysts will be discussed. The electrocatalytic activity of catalysis can be theoretically evaluated by overpotential value determined from free energy diagram (FED) of electrochemical reactions. By comparing electrocatalytic activity of systematically designed graphene-based catalysts, we will discuss the structure-catalytic activity relationships, especially the electronic and geometrical effects of heteroatom dopants.

Keywords: DFT, electrocatalysis, HER, OER, ORR, FED, overpotential, dopant, carbon

1. Introduction

With the climate change, fast consumption of fossil fuels, and environment situations due to carbon release, the research and development of clean energy is of vital importance in the coming decades. Promising applications of electrocatalysis for clean energy conversion, for example fuel cells, water electrolysis, metal-air batteries, and CO_2 to fuel conversion, are the subjects of both extensive fundamental and utilitarian studies. These technologies play a crucial role in the future of sustainable energy utilization infrastructure, and thus huge research efforts have been dedicated to improving the electrocatalytic activity of these reactions, which include electrocatalytic oxygen reduction reaction (ORR), and hydrogen oxidation reaction (HOR) that occur on the cathode and anode of a hydrogen-oxygen fuel cell, respectively, and hydrogen evolution reaction (HER) and oxygen evolution reaction (OER) at the

cathode and the anode of an electrolytic cell producing gaseous molecular hydrogen and oxygen, respectively. These reactions play an important role in regenerative fuel cells and dominate their overall performance [1–5]. Understanding the HER/OER/ORR mechanisms of various catalysts could provide design guidelines for material and process development, as well as facilitating the discovery of new catalysts. Above all, the detailed OER/ORR mechanisms in acid/alkaline environment are still being studied. Generally, OER/ORR can proceed in Langmuir-Hinshelwood (LH) or Eley-Rideal (ER) mechanisms [6]. The LH mechanism comprises all reactive intermediates on the surface while the ER mechanism includes species from the electrolyte that reacts with the surface intermediate. Despite the controversy over the mechanism, ER mechanism is generally accepted with lower reaction energy barrier than that of LH mechanism [7], and many researchers have conducted theoretical studies on OER/ORR based on the ER mechanism. However, there are two feasible reaction pathways in ER mechanism, two-step pathway and four-step pathway depending on the relative stability of O^* and OOH^* intermediates generated after the adsorption of O_2 on the catalyst [8]. Thus, we sought to describe the detailed reaction pathway of the OER/ORR as well as proposing solutions for the determination of the preferred reaction pathway on the ER mechanism.

Precious metals such as platinum (Pt), iridium (Ir), and ruthenium (Ru)-based catalysts [9–11] are generally needed to promote the HER for the generation of hydrogen fuel from the electrochemical splitting of water, the ORR in fuel cells for energy conversion, and the OER in metal-air batteries for energy storage. Besides the requirement for high catalytic activity, other issues related to these catalysts are their limited reserves and comparatively high cost, which have precluded these renewable energy technologies from large-scale commercial applications. In this regard, huge amount of efforts has been devoted to develop novel electrocatalysts to completely or partially replace precious metal catalysts in energy technologies. Along with the intensive research efforts in developing nonprecious electrocatalysts to reduce or to replace precious metal catalysts, various carbon-based, metal-free catalysts have been extensively studied because they have unique advantages for designated catalysis due to their tunable molecular structures, abundance and strong tolerance to acid/alkaline environments when used as alternative HER/OER/ORR catalysts. A rapidly growing field of metal-free catalysis based on carbon-based materials has developed, and a substantial amount of literature in both on the theoretical and experimental fields has been generated. Recent studies have revealed that graphene, [12] graphite, [13] vertically aligned nitrogen-doped carbon nanotubes (VA-NCNTs), [14] heteroatom-doped CNTs, [15] and nitrogen-doped graphene sheets [16] have excellent catalytic performance. The presence of N in N-doped graphene leads to more chemically active sites, a high density of defects and high electrochemical activity. Due to these enhanced electronic properties, N-doped catalysts in the C network are attractive for a wide range of applications, including as metal-free catalysts for HER/OER/ORR in fuel cell systems. Recently, carbon nitride-based catalysts (C_3N_4 and C_2N) with N-rich including both graphitic and pyridinic N moieties is a promising catalyst due to its competitiveness over a wide range of electrocatalyst processes, despite pure C_3N_4 and C_2N itself being inert with regard to HER/OER/ORR activity. Here, we attempted to enhance the catalytic activity of graphene, C_3N_4 and C_2N by introducing heteroatoms, which is an effective way to manipulate its electronic structure and electrochemical properties.

In this chapter, we will introduce metal-free bifunctional electrocatalysts of the heteroatom-doped graphenes (GXs, where G and X represent graphene and the heteroatom dopant) for HER [17] and the heteroatom-doped C_3N_4 (X_Y-C_3N_4s, where X and Y indicate the dopant and doping site on C_3N_4, respectively) for OER/ORR [18–20]. From the doping effect which shows better performance for HER/OER/ORR, we first present evidence that structural deformation and periodic lattice defects play the fundamental role in the HER activity of GXs by adjusting the electronic properties of graphene. We found that graphene doped with third row elements has higher HER activity with out-of-plane structural deformation compared to graphene doped with second row elements, in which graphene tends to maintain its planar structure. We systematically describe a structure-activity relationship in GXs for HER based on a thorough understanding of the effects of dopants, respectively. In addition, the third row elements-doped graphenes (GSi, GP and GS) show an interesting regularity described by a simple 3 N rule: GXs give outstanding HER activity with sustained metallic property when its primitive cell size has 3×3 N (N is integral) supercell size of pure graphene. Secondly, we describe not only the detailed OER/ORR mechanisms but also improved OER/ORR activity of C_3N_4 by introducing dopants such as P or S into the C_3N_4 matrix. Especially, we explore the causes of variation in HER/OER/ORR performance with respect to the type of dopant by comparing geometric and electronic structures of GXs and X_Y-C_3N_4s.

From these geometric and electronic structures, we demonstrated that GXs [17] and X_Y-C_3N_4 [18–20] show outstanding HER/OER/ORR activity with synergistic geometric and electronic effects, which coordinatively increase unsaturated sp^3-C via structural deformation and improve electrical conductance by modulating the electronic structure with extra electrons from dopants. Our theoretical investigations suggest that the synergistic effect between geometric and electronic factors plays an important role in HER/OER/ORR catalytic activities. It can be emphasized that there is a close correlation between the geometric/electronic structure and HER/OER/ORR catalytic activities. This understanding of the structure-activity relationship will give an insight into the development of new highly efficient electrocatalytic materials.

2. Theoretical background

2.1. Hydrogen evolution reaction

HER is a multistep process that takes place on the surface of catalyst, and there are two proposed mechanisms: Volmer-Heyrovsky and Volmer-Tafel. Both Volmer-Heyrovsky and Volmer-Tafel mechanisms describe the hydrogen atom adsorption and hydrogen molecule desorption reactions among (1) an initial state $2H^+ + 2e^-$, (2) an intermediate adsorbed state $H^* + H^+ + e^-$ or $2H^*$, and (3) a final product state $2H^+ + 2e^-$, where the $*$ and H^* denote the active site and adsorbed hydrogen atom on the surface of the catalyst, respectively. Because the initial and final states are equivalent at equilibrium reduction potential, U = 0, the Gibbs free energy of the intermediate state, $|\Delta G_{H^*}|$, has been considered as a major descriptor of the HER activity for a wide variety of catalysts. Therefore, the optimum value of $|\Delta G_{H^*}|$ should be zero for a spontaneous reaction without activation energy barrier. The Pt catalyst facilitates HER

with a low activation energy, $|\Delta G_{H^*}| \sim 0.09$ eV [21]. In this work, we have considered the Volmer-Tafel mechanism to calculate the Gibbs free energy of the intermediate state, $\Delta G_{H^*}^{Volmer}(\theta_{H1^*})$, $\Delta G_{H^*}^{Volmer}(\theta_{H2^*})$, $\Delta G_{H^*}^{Heyrovsky}(\theta_{H1^*})$, and $\Delta G_{H^*}^{Tafel}(\theta_{H2^*})$ with different hydrogen coverage at the active sites, θ_{H1^*}, and θ_{H2^*}, as shown in **Figure 1**. The Gibbs free energy of the adsorbed hydrogen is calculated as:

$$\Delta G_{H^*} = \Delta E_{H^*} + \Delta E_{ZPE} - T\Delta S_H \tag{1}$$

where ΔE_{H^*} is hydrogen adsorption energy and ΔE_{ZPE} is the difference in zero point energy (ZPE) between the adsorbed state and the gas phase. ΔS_H refers to the entropy of adsorption of $1/2 H_2$, which is the $\Delta S_H \cong -1/2 S_{H_2}^0$, where $S_{H_2}^0$ is the entropy of H_2 in the gas phase at STP. ZPE and entropic corrections, $\Delta E_{ZPE} - T\Delta S_H$ of the heteroatom-doped graphenes (GXs, where G and X represent graphene and the heteroatom dopant), are listed in **Table 1**. The hydrogen adsorption energy ΔE_{H^*} can be defined in two ways: the integral and differential H adsorption energy as a function of the H coverage in Eqs. (2) and (3), respectively.

The gas phase values were from reference 17, while the values for the adsorbed species were taken from DFT calculations. The same values for the adsorbed species for all the *N X N* models were used, as vibrational frequencies have been found to depend much less on the surface than the bond strength.

$$E_{H^*}^{int}(n) = 1/2[E(surf + nH^*) - E(surf)] - 1/2E(H_2) \tag{2}$$

$$E_{H^*}^{diff}(\theta_{H^*}) = \delta E_{H^*}^{int}(n)/\delta n = \left[E_{H^*}^{int}(n) - E_{H^*}^{int}(n-1)\right]/\Delta n \tag{3}$$
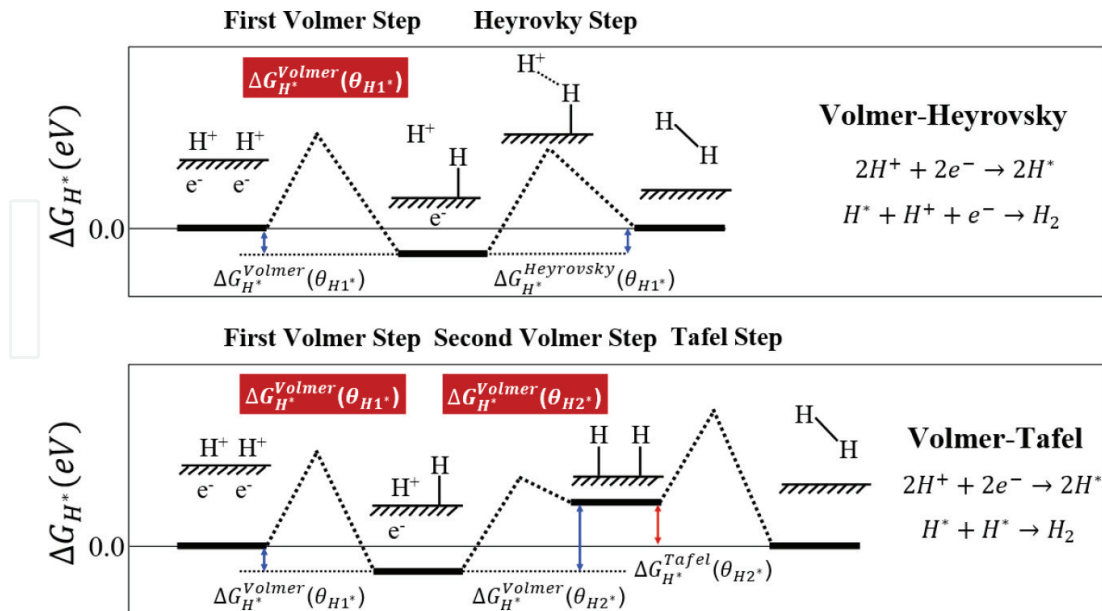
Figure 1. Schematic of Volmer-Heyrovsky and Volmer-Tafel mechanisms. $\Delta G_{H^*}^{Volmer}(\theta_{H1^*})$, $\Delta G_{H^*}^{Volmer}(\theta_{H2^*})$, $\Delta G_{H^*}^{Heyrovsky}(\theta_{H1^*})$, and $\Delta G_{H^*}^{Tafel}(\theta_{H2^*})$ are free energies of the first-, and second-Volmer steps, Hyrovsky and Tafel step, where θ_{H1^*}, and θ_{H2^*} indicate different hydrogen coverage of active sites.

eV	ZPE	TS	△ZPE	T△S	△ZPE-T△S
G-H*	0.25	–	0.11	−0.21	0.32
GB-H*	0.25	–	0.12	−0.21	0.32
GN-H*	0.29	–	0.16	−0.21	0.36
GP-H*	0.30	–	0.17	−0.21	0.37
GS-H*	0.31	–	0.18	−0.21	0.38
GSi-H*	0.30	–	0.17	−0.21	0.37
H_2	0.27	0.41	–	–	–

Table 1. Zero point energy (ZPE) and entropic (TS) correction for heteroatom doped-graphenes (G, GB, GN, GP, and GSi) at 298 K.

where n, H^* and θ_{H^*} refer to the number of hydrogen atoms, adsorbed hydrogen on the surface, and hydrogen coverage, respectively.

In contrast to the single hydrogen reaction of the Volmer step, two hydrogen atoms mediate the Tafel step. Therefore, we obtain the Gibbs free energy of the intermediate state during the Volmer and Tafel steps with the following equations to determine the different hydrogen coverages of active sites.

$$\Delta G_{H^*}^{Volmer} = \Delta E_{H^*}^{Volmer} + \Delta E_{ZPE} - T\Delta S \tag{4}$$

$$\Delta E_{H^*}^{Volmer} = E_{H^*}^{diff}(\theta_{H^*}) = [E_{H^*}^{int}(n) - E_{H^*}^{int}(n-1)]/\Delta)] \qquad \Delta n = 1 \tag{5}$$
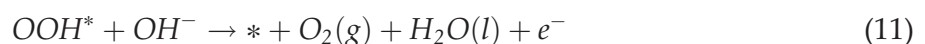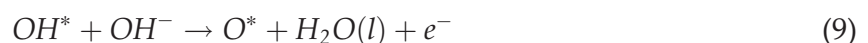
$$\Delta G_{H^*}^{Tafel} = \Delta E_{H^*}^{Tafel} + \Delta E_{ZPE} - T\Delta S \tag{6}$$

$$\Delta E_{H^*}^{Tafel} = E_{H^*}^{diff}(\theta_{H^*}) = [E_{H^*}^{int}(n-2) - E_{H^*}^{int}(n)]/\Delta n) \qquad \Delta n = 2 \tag{7}$$

2.2. Oxygen evolution reaction and oxygen reduction reaction

2.2.1. Reaction pathways in alkaline media

The generally acceptable OER mechanism is the four-electron associative mechanism in alkaline media. The four elementary steps of OER mechanism are described as follows:

$$OH^- + * \rightarrow OH^* + e^- \tag{8}$$

$$OH^* + OH^- \rightarrow O^* + H_2O(l) + e^- \tag{9}$$

$$O^* + OH^- \rightarrow OOH^* + e^- \tag{10}$$

$$OOH^* + OH^- \rightarrow * + O_2(g) + H_2O(l) + e^- \tag{11}$$

where * represents the active site on the surface, *(l)* and *(g)* refer to liquid and gas phases, respectively, and O^*, OH^* and OOH^* are adsorbed intermediates.

In contrast to OER, ORR can proceed either by a two-step or four-step pathways depending on the relative stability of O^* and OOH^* intermediates generated after the adsorption of O_2 on the catalyst. The two-step pathway of ORR in alkaline environment is summarized using the following elementary steps,

$$O_2 + H_2O(l) + 2e^- \rightarrow O^* + 2OH^- \tag{12}$$

$$O^* + 2OH^- + H_2O(l) + 2e^- \rightarrow 4OH^- \tag{13}$$

whereas the four-step pathway has following elementary steps:

$$O_2 + H_2O(l) + e^- \rightarrow OOH^* + OH^- \tag{14}$$

$$OOH^* + e^- \rightarrow O^* + OH^- \tag{15}$$

$$O^* + H_2O(l) + e^- \rightarrow OH^* + OH^- \tag{16}$$

$$OH^* + e^- \rightarrow * + OH^- \tag{17}$$

Looking at the elementary reaction steps of ORR, both reaction pathways lead to the same final products as $4OH^-$ and the different intermediate states after the adsorption of O_2 on the catalyst, O^* in (Eq. (12)) and OOH^* in (Eq. (14)). Therefore, it is worth mentioning that the transformation step of O_2^* to O^* in (Eq. (12)) or O_2^* to OOH^* in (Eq. (14)) can be important index to determine the ORR pathway.

2.2.2. Derivation of the free energy relations

The free energy change of each elementary reaction of OER in alkaline media can be expressed as follows:

$$\Delta G_1 = G_{OH^*} + \mu_{e^-} - \left(\mu_{OH^-} + G_* \right) \tag{18}$$

$$\Delta G_2 = G_{O^*} + \mu_{H_2O(l)} + \mu_{e^-} - \left(G_{OH^*} + \mu_{OH^-} \right) \tag{19}$$

$$\Delta G_3 = G_{OOH^*} + \mu_{e^-} - \left(G_{O^*} + \mu_{OH^-} \right) \tag{20}$$

$$\Delta G_4 = G_* + \mu_{O_2} + \mu_{H_2O(l)} + \mu_{e^-} - \left(G_{OOH^*} + \mu_{OH^-} \right) \tag{21}$$

Therefore, the free energy change of each elementary reaction can be calculated using (1) the chemical potentials of hydroxide, electron, liquid water and oxygen molecule (μ_{OH^-}, μ_{e^-}, $\mu_{H_2O(l)}$ and μ_{O_2}) and (2) the free energies of each intermediate (G_{OH^*}, G_{O^*}, and G_{OOH^*}) on the surface of catalyst (*). In the following paragraph, we describe the theoretical method to calculate the free energy change of each elementary reaction of the proposed reaction path based on the relation between the standard electrode potential and the chemical potential of hydroxides and electrons in alkaline environment.

2.2.3. The chemical potentials of OH^-, e^-, H_2O, and O_2

In alkaline environment, the standard oxygen reduction reaction is described as follows:

$$O_2(g) + 2H_2O(l) + 4e^- \rightarrow 4OH^- \qquad E^0 = 0.402V \qquad (22)$$

and the standard reduction potential (E^0) is 0.402 V at T = 298.15 K. In terms of chemical potentials, the equations are expressed as follows:

$$\mu_{o_2(g)} + 2\mu_{H_2O(l)} + 4\mu_{e^-} = 4\mu_{OH^-} \qquad (23)$$

$$\mu_{e^-} - \mu_{OH^-} = -1/4\left(\mu_{O_2(g)} + 2\mu_{H_2O(l)}\right) \qquad (24)$$

The left side in (Eq. (24)), the chemical potentials of electron and hydroxide, could be derived further as follows:

$$\mu_{e^-} = \mu_{e^-}^0 - eU \qquad (25)$$

$$\mu_{OH^-} = \mu_{OH^-}^0 + \kappa_B T \ln a_{OH^-} \qquad (26)$$

where eU represents the shift in electron energy when a bias is applied and $\mu_{e^-}^0$, $\mu_{OH^-}^0$ represent the chemical potentials of electron and hydroxide at standard conditions ($a_{OH^-} = 1, T = 298.15K,$ and $eU = E^0 = 0.402V$). Therefore,

$$\mu_{e^-} - \mu_{OH^-} = \left(\mu_{e^-}^0 - eU\right) - \left(\mu_{OH^-}^0 + \kappa_B T \ln a_{OH^-}\right) \qquad (27)$$

$$\mu_{e^-} - \mu_{OH^-} = \mu_{e^-}^0 - \mu_{OH^-}^0 - eU = -1/4\left(\mu_{O_2(g)} + 2\mu_{H_2O(l)}\right) \qquad (28)$$

at standard and equilibrium conditions ($a_{OH^-} = 1, T = 298.15K,$ and $eU = E^0 = 0.402V$). In the case of the right side in Eq. (24), the chemical potentials of liquid water and oxygen molecule ($\mu_{H_2O(l)}$ and $\mu_{O_2(g)}$) can be calculated from the approximations proposed by Norskov et al., where the chemical potential of liquid water ($\mu_{H_2O(l)}$) is equal to the chemical potential of water in the gas phase ($\mu_{H_2O(g)}$), at T = 298.15 K and 0.035 bars.

$$\mu_{H_2O(l)} = \mu_{H_2O(g)} = E_{DFT}^{H_2O(g)} + ZPE_{H_2O(g)} - TS_{H_2O(g)}^0 \qquad (29)$$

Moreover, the chemical potential of oxygen molecule ($\mu_{O_2(g)}$) is derived from the standard free energy change of the reaction:

$$1/2O_2(g) + H_2(g) \leftrightarrow H_2O(l) \qquad (30)$$

Because the experimental standard free energy change is -2.46 eV, the equation can be written as:

$$G_{H_2O(l)}^0 - 1/2G_{O_2(g)}^0 - G_{H_2(g)}^0 = -2.46eV \qquad (31)$$

Therefore, the chemical potential of oxygen molecule ($\mu_{O_2(g)}$) can be approximately calculated as follows:

$$\mu_{O_2(g)} = 4.92 + 2\left(E_{DFT}^{H_2O(g)} + ZPE_{H_2O(g)} - TS_{H_2O(g)}^0\right) \\ - 2\left(E_{DFT}^{H_2(g)} + ZPE_{H_2(g)} - TS_{H_2(g)}^0\right) \tag{32}$$

Therefore, Eq. (24) can be written as:

$$\mu_{e^-} - \mu_{OH^-} - eU = -1/4\left(\mu_{O_2(g)} + 2\mu_{H_2O(g)}\right) \tag{33}$$

Finally, we can obtain $\mu_{e^-}^0 - \mu_{OH^-}^0 - eU$ value as 9.952 eV using the (Eq. (29)), (Eq. (32)) and (Eq. (33)) [20]. The enthalpy change (E_{DFT}), the zero-point energy correction (Δ_{ZPE}) calculated by the DFT calculations of vibrational frequencies, and entropy corrections (TS) are listed in **Table 2**.

Gas phase H_2O at 0.035 bar was used as the reference state because at this pressure gas phase H_2O is in equilibrium with liquid water at 300 K. The same values for the adsorbed species for all the models were used, as vibrational frequencies have been found to depend much less on the surface than the bond strength. We took the standard entropies from thermodynamic tables for gas phase molecules.

2.2.4. The free energies of each intermediate (G_{OH^*}, G_{O^*}, and G_{OOH^*}) on the surface of catalyst (*)

Step 1. $OH^- + * \rightarrow OH^* + e^-$

The first step is the adsorption step of active site with a release of an electron:

$$\Delta G_1 = G_{OH^*} + \mu_{e^-} - \left(\mu_{OH^-} + G_*\right) \\ = \left(G_{OH^*} - G_*\right) + \left(\mu_{e^-}^0 - \mu_{OH^-}^0 - eU\right) \tag{34}$$

where respectively and could be expressed by DFT energies:

Species	E (eV)	ZPE (eV)	TS (eV)
H_2O (0.035 bar)	−14.22	0.56	0.67
H_2	−6.76	0.27	0.41
O*	—	0.09	0.05
OH*	—	0.41	0.07
OOH*	—	0.46	0.16

Table 2. Total energies (E) of H_2O and H_2 and zero point energy (ZPE) corrections and entropic contributions (TS) to the free energies.

$$G_{OH^*} = E_{DFT}^{OH^*} + ZPE_{OH^*} - TS_{OH^*}^0 \tag{35}$$

$$G_* = G_{OH^*} \tag{36}$$

Replacing (Eq. (33)), (Eq. (35)) and (Eq. (36)) in (Eq. (34)) we get:

$$\begin{aligned}
\Delta G_1 &= \left[\left(E_{DFT}^{OH^*} + ZPE - TS^0 \right) - E_{DFT}^* \right] + \left(\mu_{e^-}^0 - \mu_{OH^-}^0 - eU \right) \\
&= \left[\left(E_{DFT}^{OH^*} + ZPE - TS^0 \right) - E_{DFT}^* \right] + 9.952eV
\end{aligned} \tag{37}$$

Step 2: $OH^* + OH^- \rightarrow O^* + H_2O(l) + e^-$

The second step is oxidation of the OH^* species to O^* with release of water and an electron:

$$\begin{aligned}
\Delta G_2 &= G_{O^*} + \mu_{H_2O(l)} + \mu_{e^-} - \left(G_{OH^*} + \mu_{OH^-} \right) \\
&= \left(G_{O^*} + \mu_{H_2O(l)} - G_{OH^*} \right) + \left(\mu_{e^-}^0 - \mu_{OH^-}^0 - eU \right)
\end{aligned} \tag{38}$$

The relation for G_{O^*} in terms of DFT energies is similar to the relation for (Eq. (35)). Replacing again the same equations as in the case for the first step in (Eq. (38)) we get:

$$\Delta G_2 = \left[\left(E_{DFT}^{O^*} + E_{DFT}^{H_2O(g)} \right) - E_{DFT}^{OH^*} + \left(\Delta ZPE\text{-}T\Delta S^0 \right) \right] + 9.952eV \tag{39}$$

**Step 3: $O^* + OH^- \rightarrow OOH^* + e^-$**

The third step is represented by formation of the OOH^* on top of oxygen with a release of an electron:

$$\begin{aligned}
\Delta G_3 &= G_{OOH^*} + \mu_{e^-} - \left(G_{O^*} + \mu_{OH^-} \right) \\
&= \left(G_{OOH^*} - G_{O^*} \right) + \left(\mu_{e^-}^0 - \mu_{OH^-}^0 - eU \right)
\end{aligned} \tag{40}$$

The relation for G_{OOH^*} and G_{O^*} in terms of DFT energies is similar to the relation for (Eq. (35)). The same equations are replaced gradually in the (Eq. (40)) as follows:

$$\Delta G_3 = \left[E_{DFT}^{OOH^*} - E_{DFT}^{O^*} + \left(\Delta ZPE\text{-}T\Delta S^0 \right) \right] + 9.952eV \tag{41}$$

Step 4: $OOH^* + OH^- \rightarrow * + O_2(g) + H_2O(l) + e^-$
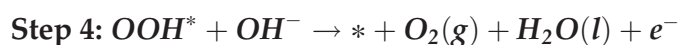
The last step is the evolution of oxygen molecule:

$$\begin{aligned}
\Delta G_4 &= G_* + \mu_{O_2(g)} + \mu_{H_2O(l)} + \mu_{e^-} - \left(G_{OOH^*} + \mu_{OH^-} \right) \\
&= \left(G_* + \mu_{O_2(g)} + \mu_{H_2O(l)} - G_{OOH^*} \right) + \left(\mu_{e^-}^0 - \mu_{OH^-}^0 - eU \right)
\end{aligned} \tag{42}$$

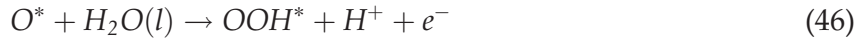Therefore, we leave from the following equation:

$$\Delta G_4 = \left[E_{DFT}^* + \left(4.92 + 2 \left(E_{DFT}^{H_2O(g)} - E_{DFT}^{H_2(g)} \right) \right) + E_{DFT}^{H_2O(g)} \right] - E_{DFT}^{OOH^*} + \left(\Delta ZPE\text{-}T\Delta S^0 \right) \right] + 9.952 eV$$

(43)

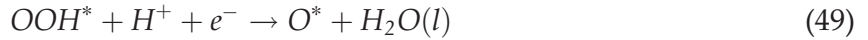Finally, the summation of ΔG_1, ΔG_2, ΔG_3, and ΔG_4 should be 1.608 eV.

The reaction free energies of O^*, OH^* and OOH^* species on the surface of catalyst are corrected by ZPE and TS. Moreover, the free energy relations of the ORR in alkaline media can also be explained in the same vein as the OER above mentioned [20].

2.2.5. Reaction pathways in acidic media

The generally acceptable OER mechanism is the four-electron associative mechanism in acidic media. The four elementary steps of OER mechanism are described as follows:

$$H_2O(l) + * \rightarrow OH^* + H^+ + e^-$$

(44)

$$OH^* \rightarrow O^* + H^+ + e^-$$

(45)

$$O^* + H_2O(l) \rightarrow OOH^* + H^+ + e^-$$

(46)

$$OOH^* \rightarrow * + O_2(g) + H^+ + e^-$$

(47)

where $*$ represents the active site on the surface, (l) and (g) refer to liquid and gas phases, respectively, and O^*, OH^* and OOH^* are adsorbed intermediates. The ORR can proceed completely via a direct four-electron process in which $O_2(g)$ is reduced directly to water H_2O (g), without involvement of hydrogen peroxide. The ORR mechanism is summarized using the following elementary steps,

$$O_2(g) + H^+ + e^- \rightarrow OOH^*$$

(48)

$$OOH^* + H^+ + e^- \rightarrow O^* + H_2O(l)$$

(49)

$$O^* + H^+ + e^- \rightarrow OH^*$$

(50)

$$OH^* + H^+ + e^- \rightarrow * + H_2O(l)$$

(51)

Here, we took the OER reactions ((44)–(47)) to derive the thermochemistry of both OER/ORR, because the ORR reactions (Eqs. ((48)–(51)) are inversed from the OER reactions (Eqs. ((44)–(47)). The catalytic activity of the OER/ORR processes can be determined by examining the reaction free energies of the different elementary steps.

2.2.6. Derivation of the free energy relations

The free energy change of each elementary reaction of OER can be expressed as follows:

$$\Delta G_1 = G_{OH^*} + \mu_{H^+} + \mu_{e^-} - \left(\mu_{H_2O(l)} + G_* \right)$$

(52)

$$\Delta G_2 = G_{O*} + \mu_{H^+} + \mu_{e^-} - (G_{OH*}) \tag{53}$$

$$\Delta G_3 = G_{OOH*} + \mu_{H^+} + \mu_{e^-} - \left(G_{O*} + \mu_{H_2O(l)} \right) \tag{54}$$

$$\Delta G_3 = G_* + \mu_{O_2(g)} + \mu_{H^+} + \mu_{e^-} - (G_{OOH*}) \tag{55}$$

Therefore, the free energy change of each elementary reaction can be calculated using (1) the chemical potentials of proton, electron, liquid water and oxygen molecule (μ_{H^+}, μ_{e^-}, $\mu_{H_2O(l)}$, and $\mu_{O_2(g)}$), and (2) the free energies of each intermediate (G_{OH*}, G_{O*}, and G_{OOH*}) on the surface of catalyst (*). In the following paragraph, we describe the theoretical method to calculate the free energy change of each elementary reaction of the proposed reaction path based on the relation between the standard electrode potential and the chemical potential of protons and electrons in acidic environment.

2.2.7. The chemical potentials of H^+, and e^-

In acidic environment, the standard hydrogen electrode is based on the redox half-cell,

$$H^+(aq) + e^- \rightarrow 1/2 H_2(g) \qquad E^0 = 0.00\ V \tag{56}$$
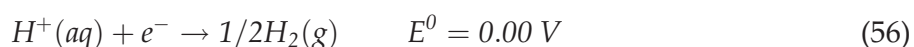
and the standard reduction potential (E^0) is 0.00 V at T = 298.15 K. In terms of chemical potentials, the equation is expressed as follows:

$$\mu_{H^+} + \mu_{e^-} = 1/2 \mu_{H_2(g)} \tag{57}$$

In (Eq. (57)), the chemical potentials of proton, electron and hydrogen could be derived further as follows:

$$\mu_{H^+} = \mu^0_{H^+} - \kappa_B T \ln a_{H^+} \tag{58}$$

$$\mu_{e^-} = \mu^0_{e^-} - eU \tag{59}$$

$$\mu_{H_2(g)} = \mu^0_{H_2} - \kappa_B T \ln p_{H_2} \tag{60}$$

where eU represents the shift in electron energy when a bias is applied and $\mu^0_{e^-}$, $\mu^0_{H^+}$ represent the chemical potentials of electron and proton at standard conditions (a_{H^+} = 1, p_{H_2} = 1bar, T = 298.15K). Therefore,

$$\mu^0_{H^+} + \mu^0_{e^-} = 1/2 \mu^0_{H_2(g)} \tag{61}$$

at standard and equilibrium conditions (a_{H^+} = 1, p_{H_2} = 1bar, T = 298.15K, and eU = E^0 = 0.00V). In the case of the right side in (Eq. (61)), we can define the standard chemical potential of hydrogen on the DFT scale from computational point of view:

$$\mu_{H_2}^0 = E_{DFT}^{H_2(g)} + ZPE_{H_2(g)} - TS_{H_2(g)}^0 \tag{62}$$

Another approximation is that for liquid water and oxygen molecule, $\mu_{H_2O(l)}$ and $\mu_{O_2(g)}$ can also be explained in the same vein as the OER in the alkaline media above mentioned.

2.2.8. The free energies of each intermediate (G_{OH^*}, G_{O^*}, and G_{OOH^*}) on the surface of catalyst (*)

Step 1: $H_2O(l) + * \rightarrow OH^* + H^+ + e^-$
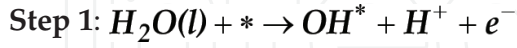
The first step is the adsorption step of OH^* on active site with a release of a proton and an electron:

$$\begin{aligned}
\Delta G_1 &= G_{OH^*} + \mu_{H^+} + \mu_{e^-} - \left(\mu_{H_2O(l)} + G_* \right) \\
&= \left(G_{OH^*} - \mu_{H_2O(l)} + G_* \right) + \left(\mu_{H^+}^0 + \mu_{e^-}^0 - eU \right)
\end{aligned} \tag{63}$$

where G_{OH^*} and G_* are expressed by DFT energies:

$$G_{OH^*} = E_{DFT}^{OH^*} + ZPE_{OH^*} - TS_{OH}^0 \tag{64}$$

$$G_* = E_{DFT}^* \tag{65}$$

Replacing (Eq. (29)), (Eq. (62)), (Eq. (64)) and (Eq. (65)) in (Eq. (63)) we get:

$$\begin{aligned}
\Delta G_1 &= \left[\left(E_{DFT}^{OH^*} - E_{DFT}^{H_2O(g)} - E_{DFT}^* \right) + \left(\Delta ZPE - T\Delta S^0 \right) \right] \\
&\quad + \left(\mu_{H^+}^0 + \mu_{e^-}^0 - eU \right) \\
&= \left[\left(E_{DFT}^{OH^*} - E_{DFT}^{H_2O(g)} - E_{DFT}^* \right) + \left(\Delta ZPE - T\Delta S^0 \right) \right] \\
&\quad + \left(1/2 E_{DFT}^{H_2(g)} - eU \right)
\end{aligned} \tag{66}$$

Step 2: $OH^* \rightarrow O^* + H^+ + e^-$
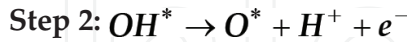
The second step is oxidation of the OH^* species to O^* with release of a proton and an electron:

$$\begin{aligned}
\Delta G_2 &= G_{O^*} + \mu_{H^+} + \mu_{e^-} - G_{OH^*} \\
&= (G_{O^*} - G_{OH^*}) + \left(\mu_{H^+}^0 + \mu_{e^-}^0 - eU \right)
\end{aligned} \tag{67}$$

The relation for G_{O^*} in terms of DFT energies is similar to the relation for (Eq. (64)). Replacing again the same equations as in the case for the first step in (Eq. (66)), we get:

$$\Delta G_2 = \left[\left(E_{DFT}^{O^*} - E_{DFT}^{OH^*} \right) + \left(\Delta ZPE - T\Delta S^0 \right) \right] + \left(1/2 E_{DFT}^{H_2(g)} - eU \right) \tag{68}$$

Step 3: $O^* \rightarrow OOH^* + H^+ + e^-$

The third step is represented by formation of the O^* on top of oxygen with a release of a proton and an electron:

$$\Delta G_3 = G_{OOH^*} + \mu_{H^+} + \mu_{e^-} - G_{O^*}$$
$$= (G_{OOH^*} - G_{O^*}) + \left(\mu_{H^+}^0 + \mu_{e^-}^0 - eU\right) \tag{69}$$

The relation for G_{OOH^*} and G_{O^*} in terms of DFT energies is similar to the relation for (Eq. (64)). The same equations are replaced gradually in the (Eq. (69)) as follows:

$$\Delta G_3 = \left[\left(E_{DFT}^{OOH^*} - E_{DFT}^{O^*}\right) + \left(\Delta ZPE\text{-}T\Delta S^0\right)\right] + \left(1/2E_{DFT}^{H_2(g)} - eU\right) \tag{70}$$

Step 4: $OOH^* \rightarrow * + O_2(g) + H^+ + e^-$

The last step is the evolution of oxygen molecule:

$$\Delta G_4 = G_* + \mu_{O_2(g)} + \mu_{H^+} + \mu_{e^-} - G_{OOH^*}$$
$$= \left(G_* + \mu_{O_2(g)} - G_{OOH^*}\right) + \left(\mu_{H^+}^0 + \mu_{e^-}^0 - eU\right) \tag{71}$$

Therefore, we leave from the following equation:

$$\Delta G_4 = \left[E_{DFT}^* + \left(4.92 + 2\left(E_{DFT}^{H_2O(g)} - E_{DFT}^{H_2(g)}\right)\right) + E_{DFT}^{OOH^*}\right]$$
$$+ \left(\Delta ZPE - T\Delta S^0\right) + \left(1/2E_{DFT}^{H_2(g)} - eU\right) \tag{72}$$

Finally, the summation of ΔG_1, ΔG_2, ΔG_3, and ΔG_4 should be 4.92 eV.

The reaction free energies of OH^*, O^* and OOH^* species on the surface of catalyst considered by ZPE and TS. Moreover, the free energy relations of the ORR in acidic media can also be explained in the same vein as the OER above mentioned.

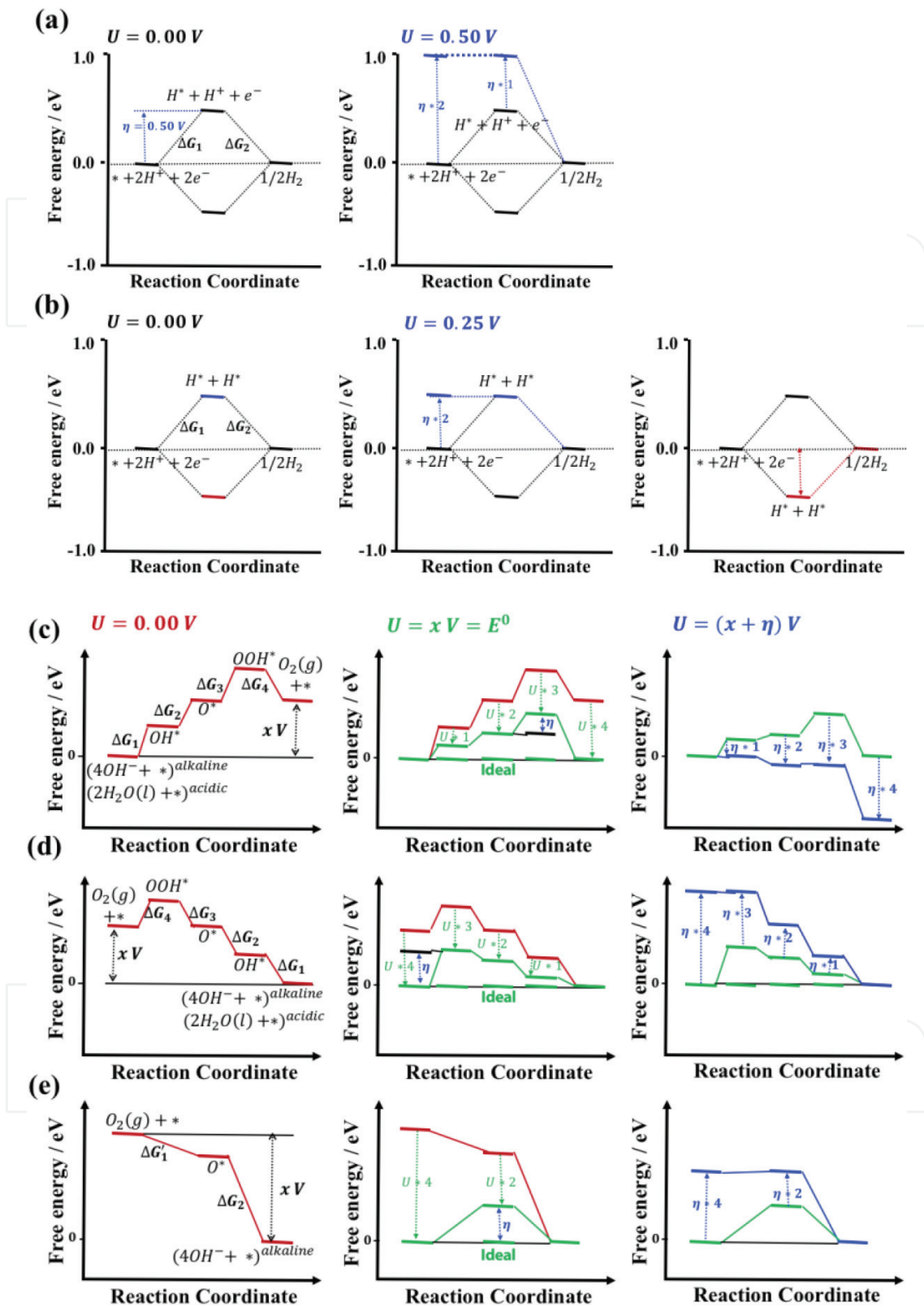## 2.3. Free energy diagram (FED) and Overpotential(η)

We can deduce an important parameter of electrocatalytic activity from the calculated ΔG, the magnitude of the potential-determining step (G^{HER} and $G^{OER/ORR}$) in consecutive reaction steps. This is the specific reaction step with the largest ΔG in the HER and OER/ORR elementary reaction steps, that is, the concluding step to achieve a downhill reaction in the free energy diagram (FED) with increasing potential N, as shown in **Figure 2** for HER and **Figure 3** for OER/ORR:

$$G^{HER} = max\left[\Delta G_1^0, \Delta G_2^0\right] \tag{73}$$

$$G^{OER/ORR} = max\left[\Delta G_1^0, \Delta G_2^0, \Delta G_3^0, \Delta G_4^0\right] \tag{74}$$

$$G^{ORR} = max\left[\Delta G_1^0, \Delta G_2^0\right] \tag{75}$$

Figure 2. Free energy diagrams (FEDs) of (a) Volmer-Heyrovsky pathway and (b) Volmer-Tafel pathway for HER, and (c) four-step associative OER pathway, and (d) four-step ORR pathway in alkaline/acidic media, and (e) two-step ORR pathway in alkaline media at zero potential ($U = 0\ V$), at equilibrium reduction potential ($U = x\ V$) and at overpotential ($U = (x + \eta\ V)$. The x values indicate 0.402 V (alkaline) or 1.230 V (acidic).
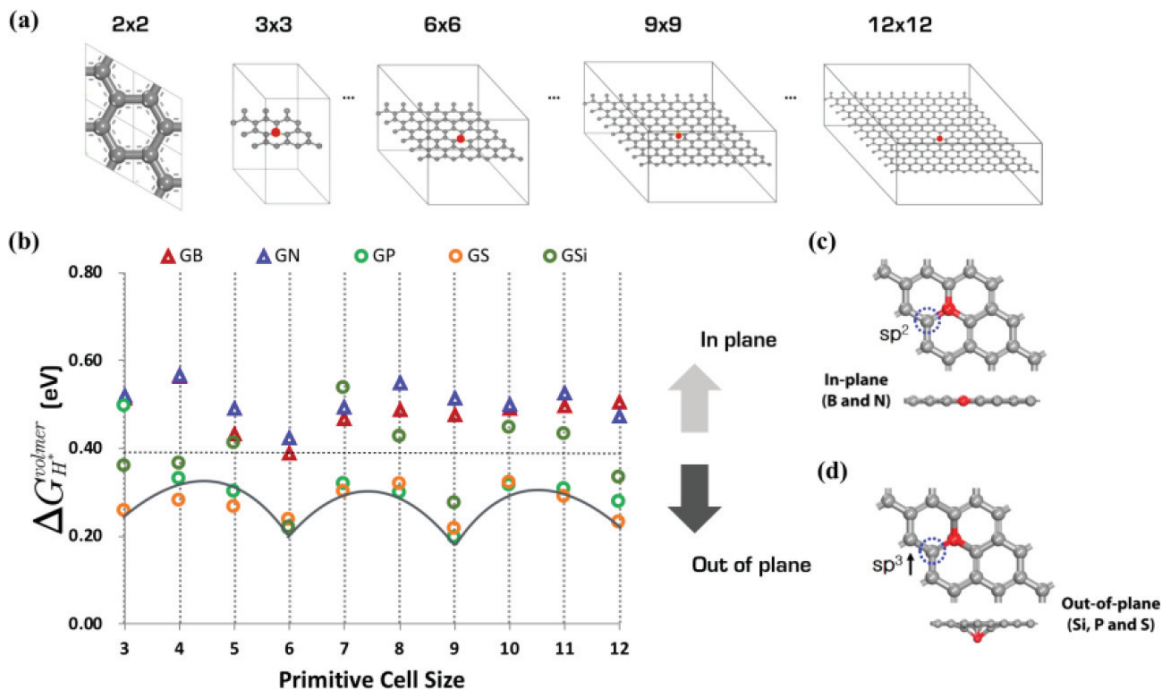
Figure 3. (a) Primitive cells of single heteroatom doped-graphene (GX, where G means graphene and X is B, N, Si, P, and S dopant) and (b) HER activities ΔG^{Volmer} of GX as a function of primitive cell size. Red mark indicates dopant. There are two different types of structures depending on dopant, (c) in-plane and (d) out-of-plane.

The theoretical overpotential at standard conditions is then given by (Eq. (76)) in acidic and alkaline conditions, respectively:

$$\eta^{HER} = \left(G^{HER}/e\right) - x\ V, \quad x = 0.000\ V \tag{76}$$

$$\eta^{OER/ORR} = \left(G^{OER/ORR}/e\right) - x\ V,$$
$$x = 1.230\ V\ (acidic), \quad \text{and}\ 0.402\ V(alkaline) \tag{77}$$

In the case of HER pathways, the Volmer-Heyrovsky reaction is an electrochemical reaction involving electrons at all steps, as shown in **Figure 2(a)**. Therefore, when the external potential $(U = 0.50V)$ is applied, the chemical potential of steps involving electrons shifts by the external potential $(U = 0.50V)$, and the Volmer-Heyrovsky reaction changes from uphill to downhill reaction. In contrast to the Volmer-Heyrovsky reaction, the Volmer-Tafel reaction is an electrochemical reaction involving electrons only in the Volmer step, as shown in **Figure 2(b)**. Therefore, when the adsorption of hydrogen is unstable, the downhill reaction is possible by applying the external potential $(U = 0.25V)$, but when the adsorption of hydrogen is stable, the reduction of H^+ is spontaneous reaction, and the desorption of H_2 in the Tafel step is the rate determining step. However, the desorption of H_2 is a thermodynamic reaction, which is not involved in electrons, not an electrochemical reaction. In the case of OER/ORR pathways, the theoretical overpotential $(\eta^{OEP/OPP})$ represents the relative stability of the intermediates between $(4OH^- + *)^{alkaline}$, $(2H_2O(l) + *)^{acidic}$ and $(O_2(g) + *)$, and vice versa, as shown in **Figure 2 (c)-(e)**. In addition, it can be calculated by applying standard density functional theory (DFT)

in combination with the computational standard hydrogen electrode (SHE) model. Because the equilibrium reduction potential is *U = 1.230 V (acidic)* and *0.402 V(alkaline)*, the chemical potential difference between *(4OH⁻)^(alkaline)*, *(2H₂O(l))^(acidic)* and *O₂(g)* should be 1.608 and 4.920 V, respectively. However, the actual catalytic behaviors deviate from the ideal case due to correlation with binding energies of the intermediates. Therefore, most catalysts require overpotential (η^{HER} and $\eta^{OER/ORR}$) in order to achieve an overall downhill reaction. Consequently, the η^{HER} and $\eta^{OER/ORR}$ the important indicators of catalytic activities of a catalyst, and the lower η^{HER} and $\eta^{OER/ORR}$ indicate a thermodynamically superior catalyst.

3. Structure-catalytic activity relationships

3.1. Heteroatom doped graphene (GX) for HER catalyst

Figure 3 shows a schematic of the heteroatom doped-graphene (GX, where G means graphene and X is B, N, Si, P, and S dopant) structures. We have used the second row elements (B and N) and the third row elements (Si, P, and S) in the periodic table in order to investigate the structural and electronic doping effects on HER activity because the third row elements are relatively larger than the second row elements and p- and n-type doping effects can be expected from the electron deficient B, and electron rich N, P, and S elements give in-plane and out-of-plane structures, respectively, due to the size of the dopants.

3.1.1. Structural and electronic doping effects on HER activity

On the atomic orbital hybridization characters of adjacent carbon atoms of dopant, the natural bond orbital (NBO) analysis show an increased p orbital contribution from sp² to sp³ hybridization of carbons adjacent to the dopant due to structural deformation from in-plane to out-of-plane. Compared to sp²-hybridized carbon, sp³-hybridized carbons more readily form an extra a hydrogen atom without additional structural change. Therefore, in out-of-plane structures, the subsequent two hydrogen atoms prefer to bind to only sp³ hybridized carbons adjacent to the dopant. However, in the case of in-plane structures having only sp²-hybridized carbons, the first hydrogen atom should result in structural deformation to form sp³-hybridized carbons. Therefore, the first hydrogen adsorption on the in-plane structure is less favorable than the reaction on out-of-plane structures. The second hydrogen atom can favorably bind to sp³-hybridized second neighboring carbons of dopant. Consequently, structural deformation with dopants that are third row elements is associated with improved HER activity due to atomic orbital hybridization, as shown in **Figure 3(b)**. Looking at the electronic structures of GXs, p- and n-type doping effects are also expected from electron deficient and rich elements. In the case of in-plane GXs, electron deficient boron shifts its band structure up by withdrawing an electron from graphene, and electron rich nitrogen shifts its band structure down by donating an electron to graphene. Interestingly, in the case of out-of-plane GXs, electron rich phosphorous and sulfur dopant have no associated band shift. The origin of the flat band can be understood based on the localization of an extra electron onto the dopant site. In order to verify the relationship between geometric and electronic structures of GXs, we have

systematically changed the structures of GXs from in-plane to out-of-plane structures and vice versa. These calculations clearly show that dopant can produce n- and p-type doping states as well as a localized state depending on the structure of GXs induced by the type of dopants. When the out-of-plane (in-plane) deformation is applied in the in-plane (out-of-plane) GXs, band structures change from the p-type doping state (localized state) to the localized state (p-type doping state). Therefore, it is worth mentioning that the localized electronic states can be associated with physical regularity of HER activities on the out-of-plane GXs.

3.2. Heteroatom doped C_3N_4 (X_Y-C_3N_4) for OER/ORR bi-functional catalyst

In this work, we have systematically investigated a metal-free bifunctional electrocatalyst of heteroatom-doped carbon nitride (X_Y-C_3N_4, where X and Y indicate the dopant and doping site on C_3N_4, respectively) for oxygen evolution and oxygen reduction reactions (OER and ORR) in alkaline media, considering the possible reaction pathways based on the Eley-Rideal (ER) mechanism as well as the doping effects on electrocatalytic activity. Moreover, we determined that the relative stability of O^* and OOH^* intermediates was a key factor determining the ORR pathway; accordingly, ORR follows a two-step reaction pathway governed by O^* rather than a four-step reaction pathway governed by OOH^*. Firstly, we calculated relative E_f and the most stable structures of heteroatom-doped C_3N_4 structures, X_Y-C_3N_4, where X = P, S, or PS and Y = C or N [18, 20]. By considering the E_f (formation energy) results as well as the various doping sites, we determined the most stable X_Y-C_3N_4 structures, P_{CA}-C_3N_4, P_{NB}-C_3N_4, S_{CB}-C_3N_4, S_{NB}-C_3N_4, $P_{CA}S_{CB}$-C_3N_4, $P_{NA}S_{NB}$-C_3N_4, and $P_{CA}S_{NB}$-C_3N_4, for the investigation of OER/ORR bifunctional electrocatalytic activities and their reaction mechanisms in alkaline media.

3.2.1. OER and ORR catalytic activity on X_Y-C_3N_4

Figure 4 (a) and **(c)** show the volcano plot of OER and ORR in alkaline media at all possible active sites on X_Y-C_3N_4, which represents the apparent catalytic activity, respectively. This theoretical analysis reveals that the P_CS_C-C_3N_4 structure has minimum η^{OER} (0.42 V) and η^{ORR} (0.27 V). The $\eta^{OER/ORR}$ value of P_CS_C-C_3N_4 is comparable to those of the best conventional catalysts (~0.42 V for OER on RuO_2 and ~0.45 V for ORR on Pt). Most elementary steps in OER have an uphill reaction at 0.00 V and at equilibrium potential of 0.402 V. Analyzing the FED at the equilibrium potential of 0.402 V, we can define the rate determination step as the formation of OOH^* from O^* on P_CS_C-C_3N_4, as shown in **Figure 4 (b)**. Therefore, the ΔG at the rate determination step, 0.42 V, become the η^{OER} for facilitating the OER as a spontaneously downhill reaction. By applying the increased electrode potential of 0.82 V, all elementary reactions can be downhill reactions for spontaneous OER. In the case of the ORR, we considered the O_2 adsorption free energy ($\Delta G_{O2}*$) and η^{ORR} are highly correlated to determine ORR activity. If the O_2 adsorption reaction is very difficult to achieve as an initiation step in ORR, that material cannot have ORR activity, even though it can have a possibility to have a very small η^{ORR}. Therefore, we defined a new indicator of ORR activity as figure of merit (FOM), which is defined by $FOM = -(\eta^{ORR} + \Delta G_{O2}*)$. Using FOM, we constructed a volcano plot of ORR at all possible active sites on X_Y-C_3N_4 in order to compare the ORR catalytic activity, as shown in **Figure 4 (c)**, where the P_CS_C-C_3N_4 structure have minimum η^{ORR} of 0.27 V.
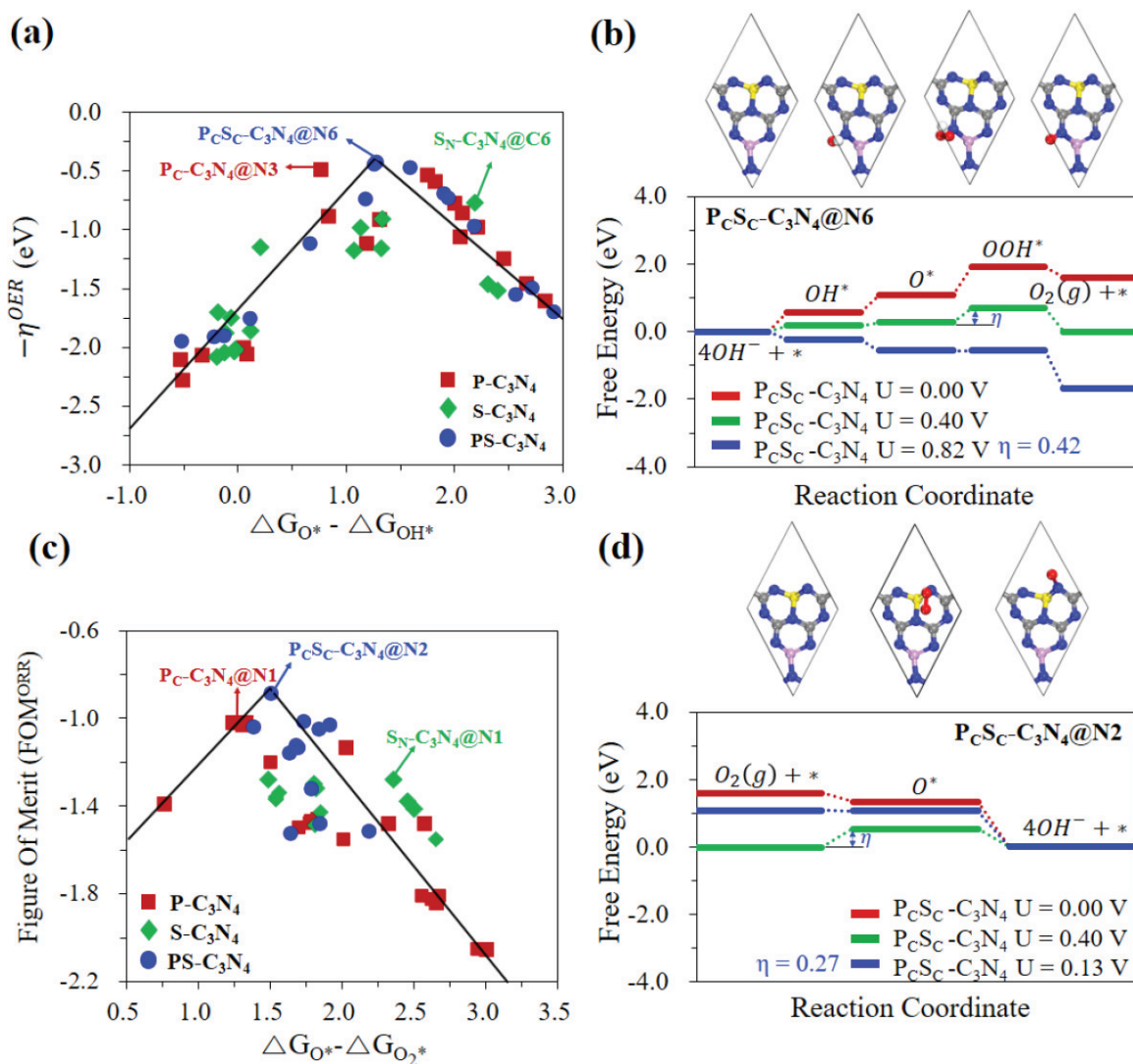
Figure 4. The volcano plots of (a) OER and (c) ORR at all possible active sites on X_Y-C_3N_4 and the free energy diagrams (FEDs) of P_CS_C-C_3N_4 structure having the best catalytic activity.

3.2.2. Structural and electronic doping effects on OER/ORR activity

The synergistic effect of P, S co-doping can be explained based on the geometric and electronic effects of heteroatoms [17–20]. Considering the atomic size of heteroatoms, the relatively larger S and P dopants can cause structural deformation of X_Y-C_3N_4, which improves the OER and ORR activity by enhancing the stability of intermediates with increasing p orbital character of active sites adjacent to the dopant from sp^2 to sp^3 hybridization. Compared to sp^2 hybridized orbitals on pure C_3N_4, sp^3 character of active sites on X_Y-C_3N_4 is more suitable for forming chemical bonds with intermediate species. Therefore, in out-of-plane structures, the intermediates prefer to bind to sp^3-hybridized active sites. Moreover, to verify the relationship between geometric and electronic structures of X_Y-C_3N_4, we intentionally changed the structures of X_Y-C_3N_4 from in-plane to out-of-plane to increase the activity for binding intermediate species by increasing the sp^3 character of active sites on X_Y-C_3N_4. We investigated density of state (DOS) of pure C_3N_4 and X_Y-C_3N_4 (X = P, S, or PS and Y = N) to determine at what condition the OER/ORR exhibit outstanding performance [18, 20]. It can be expected that

electron-rich heteroatom doping will induce electronic structure changes from a non-metallic doping effect to a metallic doping effect due to a downward band shift. As a result, P_CS_C-C_3N_4 shows the best OER/ORR activity by maintaining a metallic property despite the presence of out-of-plane deformation. Consequently, it can be emphasized that there is a close correlation between the electronic/geometric structure and OER/ORR catalytic activities, and the best bifunctional OER/ORR catalytic activity of P,S co-doped P_CS_C-C_3N_4 is attributed to a synergistic effect between the electronic and geometric effects.

4. Conclusion

We have systematically investigated the detailed mechanisms of HER/OER/ORR and the synergistic effect between geometric and electronic factors plays an important role in HER/OER/ORR catalytic activities of GXs and X_Y-C_3N_4. In this work, we demonstrated that the HER/OER/ORR activity of GXs and X_Y-C_3N_4 can be modulated by structural and electronic factors, including structural deformation with dopants. These structural and electronic factors enhance adsorbent binding strength during the reactions in HER/OER/ORR by generating sp^3-hybridized atoms and facilitating charge transfer between adsorbents and GXs/X_Y-C_3N_4 as metallic properties. Additionally, we re-evaluated the generally accepted ER mechanism of OER/ORR by comparing the stability of intermediates governing the reactions, where we found that the OER/ORR respectively follows four-step and two-step reaction pathway. We also elucidated the importance of the O_2 adsorption free energy $(\Delta G_{O2}{}^*)$ in ORR activity. Considering the $\Delta G_{O2}{}^*$ with a FOM, $FOM = -(\eta^{ORR} + \Delta G_{O2}{}^*)$, we successfully represented the ORR activity of X_Y-C_3N_4. We believe that the understanding of the detailed mechanism as well as the relationship of structure-electrocatalytic activity of the HER/OER/ORR can facilitate development of new electrocatalytic materials.

Acknowledgements

Author details

Chi Ho Lee[1] and Sang Uck Lee[1,2]*

*Address all correspondence to: sulee@hanyang.ac.kr

1 Bionano Technology, Hanyang University, Ansan, Korea

2 Chemical and Molecular Engineering, Hanyang University, Ansan, Korea

References

[1] Jiao Y, Zheng Y, Jaroniecb M, Qiao SZ. Chemical Society Reviews. 2015;**44**:2060-2086. DOI: 10.1039/c4cs00470a

[2] Chuangang H, Dai L. Angewandte Chemie, International Edition. 2016;**55**:11736-11758. DOI: 10.1002/anie.201509982

[3] Shinagawa T, Garcia-Esparza AT, Takanabe K. Scientific Reports. **5**:13801. DOI: 10.1038/srep13801

[4] Yi C, Jiang SP. Progress in Natural Science: Materials International. 2015;**25**:545-553. DOI: 10.1016/j.pnsc.2015.11.008

[5] Li J, Zheng G. Advancement of Science. 2017;**4**:1600380. DOI: 10.1002/advs.201600380

[6] Zhang P, Xiao BB, Hou XL, Zhu YF, Jiang Q. Scientific Reports. 2014;**4**:3821. DOI: 10.1038/srep03821

[7] Keith JA, Jerkiewicz G, Jacob T. Chemphyschem. 2010;**11**(13):2779-2794. DOI: 10.1002/cphc.201000286

[8] Dai L, Xue Y, Qu L, Choi HJ, Baek JB. Chemical Reviews. 2015;**115**(11):4823-4892. DOI: 10.1021/cr5003563

[9] Fabbri E, Habereder A, Waltar K, Kotz R. Catalysis Science & Technology. 2014;**4**(11):3800-3821. DOI: 10.1039/C4CY00669K

[10] Reier T, Oezaslan M, Strasser P. ACS Catalysis. 2012;**2**(8):1765-1772. DOI: 10.1021/cs3003098

[11] Lim DH, Wilcox J. Journal of Physical Chemistry C. 2012;**116**(5):3653-3660. DOI: 10.1021/jp210796e

[12] Li YF, Li M, Jiang LQ, Lin L, Cui LL, He XQ. Physical Chemistry Chemical Physics. 2014;**16**(42):23196-23205. DOI: 10.1039/C4CP02528H

[13] Sidik RA, Anderson AB, Subramanian NP, Kumaraguru SP, Popov BN. The Journal of Physical Chemistry. B. 2006;**110**(4):1787-1793. DOI: 10.1021/jp055150g

[14] Gong KP, Du F, Xia ZH, Durstock M, Dai LM. Science. 2009;**323**(5915):760-764. DOI: 10.1126/science.1168049

[15] Yang LJ, Jiang SJ, Zhao Y, Zhu L, Chen S, Wang XZ, Wu Q, Ma J, Ma YW, Hu Z. Angewantde Chemie International Edition. 2011;**50**(31):7132-7135. DOI: 10.1002/anie.201101287

[16] Li MT, Zhang LP, Xu Q, Niu JB, Xia ZH. Journal of Catalysis. 2014;**314**:66-72. DOI: 10.1016/j.jcat.2014.03.011

[17] Lee CH, Jun B, Lee SU. RSC Advances. 2017;**7**(43):27033-27039. DOI: 10.1039/C7RA04115B

[18] Shinde SS, Lee CH, Sami A, Kim DH, Lee SU, Lee JH. ACS Nano. 2017;**11**:347-357. DOI: 10.1021/acsnano.6b05914

[19] Shinde SS, Lee CH, Yu JY, Kim DH, Lee SU, Lee JH. ACS Nano. 2018;**12**:596-608. DOI: 10.1021/acsnano.7b07473

[20] Lee CH, Jun B, Lee SU. ACS Sustainable Chemistry & Engineering. 2018;**6**:4973-4980. DOI: 10.1021/acssuschemeng.7b04608

[21] Norskov JK, Bligaard T, Logadottir A, Kitchin JR, Chen JG, Pandelov S, Stimming U. Journal of the Electrochemical Society. 2005;**152**:J23-J26. DOI: 10.1149/1.1856988